

# Spectroscopic Observations of the Intermediate Polar EX Hydrae in Quiescence

N. Mhlahlo<sup>1,2\*</sup>, D.A.H. Buckley<sup>2</sup>, V.S. Dhillon<sup>3</sup>, S.B. Potter<sup>2</sup>, B. Warner<sup>1</sup> and P.A. Woudt<sup>1</sup>

<sup>1</sup>*Astronomy Department, University of Cape Town, Rondebosch 7700, Cape Town, South Africa*

<sup>2</sup>*South African Astronomical Observatory, Observatory 7935, Cape Town, South Africa*

<sup>3</sup>*Physics and Astronomy Department, University of Sheffield, Sheffield, S3 7RH, UK*

11 February 2013

## ABSTRACT

Results from spectroscopic observations of the Intermediate Polar (IP) EX Hya in quiescence during 1991 and 2001 are presented. Spin-modulated radial velocities consistent with an outer disc origin were detected for the first time in an IP. The spin pulsation was modulated with velocities near  $\sim 500 - 600 \text{ km s}^{-1}$ . These velocities are consistent with those of material circulating at the outer edge of the accretion disc, suggesting corotation of the accretion curtain with material near the Roche lobe radius. Furthermore, spin Doppler tomograms have revealed evidence of the accretion curtain emission extending from velocities of  $\sim 500 \text{ km s}^{-1}$  to  $\sim 1000 \text{ km s}^{-1}$ . These findings have confirmed the theoretical model predictions of King & Wynn (1999), Belle et al. (2002) and Norton et al. (2004) for EX Hya, which predict large accretion curtains that extend to a distance close to the Roche lobe radius in this system.

Evidence for overflow stream of material falling onto the magnetosphere was observed, confirming the result of Belle et al. (2005) that disc overflow in EX Hya is present during quiescence as well as outburst.

It appears that the H $\beta$  and H $\gamma$  spin radial velocities originated from the rotation of the funnel at the outer disc edge, while those of H $\alpha$  were produced due to the flow of material along the field lines far from the white dwarf (narrow component) and close to the white dwarf (broad-base component), in agreement with the accretion curtain model.

**Key words:** accretion discs, binary - stars: cataclysmic variables.

## 1 INTRODUCTION

EX Hya is an Intermediate Polar (IP), a sub-class of magnetic Cataclysmic Variable Stars (mCVs) where a late-type main sequence star transfers material to the magnetic white dwarf star as the two stars orbit each other under the influence of their mutual gravitation. Unlike in Polars, another subclass of mCVs, where the white dwarf is in synchronous rotation with the binary rotation ( $P_{\text{spin}} = P_{\text{orb}}$ ), the white dwarf in an IP is in asynchronous rotation with the orbital motion of the system. EX Hya, however, is nearer synchronism than the majority of IPs as it has a spin period ( $\sim 67.03 \text{ min}$ ) which is about  $2/3$  its orbital period ( $98.26 \text{ min}$ ) (Mumford 1967; Hellier et al. 1987), and is one of only six out of thirty nine confirmed IPs with its orbital period below the 2-3 h CV period gap (Norton et al. 2004). It has an inclination  $i = 78^\circ \pm 1^\circ$ .

Recent studies have shown that EX Hya does not conform to the traditional IP model (King & Wynn 1999; Wynn 2000; Belle et al. 2002; Norton et al. 2004; Belle et al. 2005). This sys-

tem has a large  $P_{\text{spin}}/P_{\text{orb}}$  ratio ( $\sim 0.68$ ) implying that it cannot be in the usual spin equilibrium rotation since most IPs have been shown to attain spin equilibrium near  $P_{\text{spin}}/P_{\text{orb}} \sim 0.1$  (King & Wynn 1999; Wynn 2000). This further implies that the corotation radius is far greater than the circularisation radius ( $R_{\text{co}} \gg R_{\text{cir}}$ ) and that EX Hya cannot possess a Keplerian disc. Systems with Keplerian discs are expected to have  $R_{\text{co}} < R_{\text{cir}}$  and thus a smaller  $P_{\text{spin}}/P_{\text{orb}}$ . These factors have prompted theorists to suggest that the spin equilibrium state in EX Hya is determined by  $R_{\text{co}} \sim b$ , where  $b$  is the distance to the inner Lagrangian point,  $L_1$  (King & Wynn 1999; Wynn 2000; Norton et al. 2004). In this model the accretion curtains extend to near the  $L_1$  point, and EX Hya resembles an asynchronous Polar where most of the material accretes via the stream (King & Wynn 1999; Wynn 2000) and via both the ring of material near the Roche lobe radius of the primary and the stream (Norton et al. 2004), depending on the orbital and spin periods of the system, and the magnetic field strength. In the later publication it was shown that material in EX Hya is fed from a ring of material at the outer edge of the Roche lobe, and that for

\* E-mail: nceba@circinus.ast.uct.ac.za

Date	HJD (start)	Time	Spectra
24-04-91	2448371.3884097	3.28	90
25-04-91	2448372.3603850	2.93	72
29-04-91	2448376.2402973	7.00	100
24-03-01	2451993.5427099	2.79	42
25-03-01	2451994.3581177	3.77	56
25-03-01	2451994.5147196	3.96	66
26-03-01	2451995.4360089	1.94	48
26-03-01	2451995.5412087	2.92	50

**Table 1.** Table of spectroscopic observations during quiescence in 1991 and 2001. The column **Date** denotes the date at the beginning of the observing night (before midnight), the column **Time** denotes the number of observing hours and **Spectra** the number of spectra obtained.

the  $P_{\text{spin}}/P_{\text{orb}}$  of EX Hya, this mode of accretion is preferred over stream-fed accretion.

In this work we present spectroscopic data of EX Hya in quiescence obtained from the SAAO in 1991 (just before EX Hya went into outburst, and a day or two after outburst) and in 2001. Outburst data of 1991 will be discussed in a later publication.

## 2 OBSERVATIONS AND DATA REDUCTION

### 2.1 1991 Observations

EX Hya was observed in April of 1991 by Buckley et al. (1991) using the SAAO 1.9-m telescope with the Reticon photon counting system (RPCS) detector on the Cassegrain spectrograph. A grating with a resolution of  $1200 \text{ mm}^{-1}$  was used and a wavelength range of  $4000 - 5080 \text{ \AA}$  was covered at a spectral resolution of  $\Delta\lambda \sim 1.2 \text{ \AA}$  and at a time resolution of  $100 - 120 \text{ s}$ . The spectrograph slit width was  $250 \text{ \mu m}$  ( $\sim 1.5$  arcsecs). Wavelength calibration exposures were taken using a CuAr arc lamp. Three nights of observations (24, 25 and 29 April 1991) were covered in quiescence and, in total, 262 spectra were obtained. The observing log is given in Table 1 together with the starting times of the observations.

Following wavelength-calibration and sky-subtraction, the data were flux calibrated using the spectra of the standard star LTT3864.

### 2.2 2001 Observations

The 2001 observations were obtained using the SiTe CCD detector ( $266 \times 1798$  pixels) on the Cassegrain spectrograph of the SAAO 1.9-m telescope. A grating with a resolution of  $1200 \text{ mm}^{-1}$  was used over the wavelength range  $4200 - 5100 \text{ \AA}$  on the nights of the 25th and 26th April. Another grating with a resolution of  $1200 \text{ mm}^{-1}$  was used on the 24th, 25th and 26th April over the range  $6300 - 7050 \text{ \AA}$ . The spectral resolution was  $\sim 1.0 \text{ \AA}$  and a  $1 \times 2$  binning scheme was employed (i.e. binning by  $2 \times$  in the spatial direction). The exposure times during observations were  $60 \text{ s}$ . The observations covered the period 24 April - 26 April 2001 and, in total, 262 spectra were obtained (Table 1). The extraction and reduction of the data were performed the standard way using the Image Reduction and Analysis Facility (IRAF)<sup>1</sup> package and the

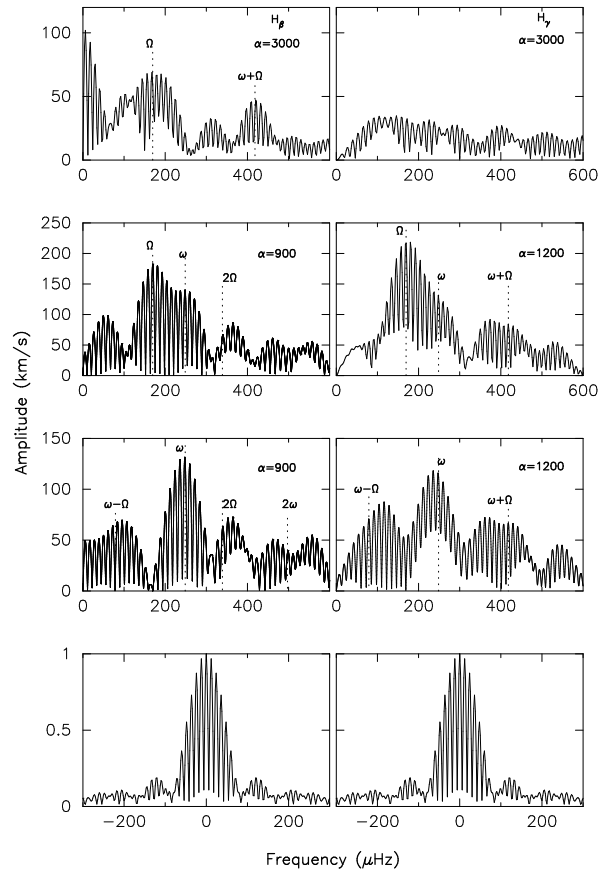


**Figure 1.** Radial-velocity Fourier amplitude spectra from the 1991 combined data are shown for  $\alpha = 3000 \text{ km s}^{-1}$  and  $900 \text{ km s}^{-1}$  for the  $\text{H}\beta$  line (top left panel and second left panel from the top) and for  $3000 \text{ km s}^{-1}$  and  $1200 \text{ km s}^{-1}$  for the  $\text{H}\gamma$  line (top right panel and second right panel from the top).  $\Omega$  denotes the orbital frequency of the system,  $2\Omega$  its first harmonic and  $\omega + \Omega$  the upper orbital side band where  $\omega$  is the spin frequency. The data were prewhitened by the orbital frequency and are displayed in the third panels from the top. Window spectra are plotted below the amplitude spectra (bottom panels).

spectra were flux calibrated using observations of the standard star LTT3218.

## 3 THE RADIAL VELOCITIES

It is widely accepted that in a canonical CV, the high velocity emission line wings are formed in the inner parts of the accretion disc orbiting close to the white dwarf and thus should reflect its orbital motion (Shafter 1983; Shafter & Szkody 1984; Shafter 1985). In IPs, however, high velocity emission line wings are formed in the gas streaming towards the white dwarf at high velocities (Hellier et al. 1987; Ferrario & Wickramasinghe 1993). The radial velocities were determined by measuring the wings of the  $\text{H}\beta$  and  $\text{H}\gamma$  emission lines from the 1991 data (24 and 25/04/91 - the data obtained on the 29th was not added since EX Hya had not fully recovered from outburst); and the wings of  $\text{H}\alpha$ ,  $\text{H}\beta$  and  $\text{H}\gamma$  emission lines from the 2001 data using the Gaussian Convolution

<sup>1</sup> IRAF is a software package for the reduction and analysis of astronomical data distributed by National Optical Astronomy Observatory (NOAO)

which is operated by the Association of Universities for Research in Astronomy (AURA)

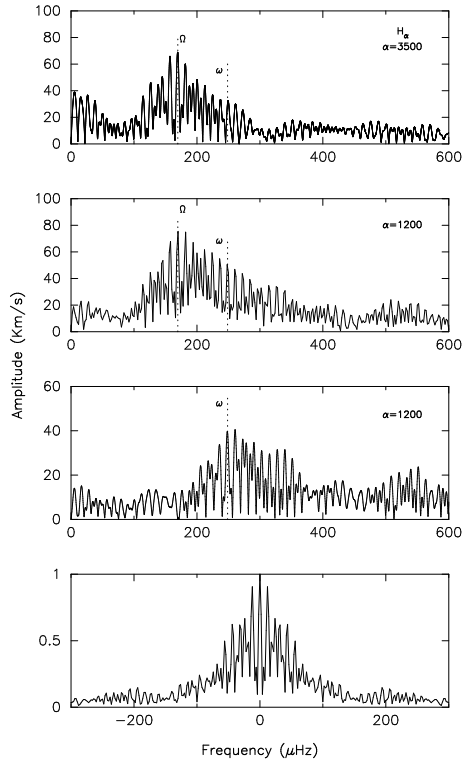


**Figure 2.** Radial velocity amplitude spectra shown for the H $\alpha$  line from 2001, for  $\alpha = 3500$  km s $^{-1}$  and 1200 km s $^{-1}$ . The vertical dashed line shows the expected position of the orbital and spin period peaks. The data were prewhitened by  $\Omega$  and are shown in the third panel from the top. A window spectrum is shown at the bottom.

Scheme (GCS, Schneider & Young 1980; Shafter & Szkody 1984; Shafter 1985). The GCS method convolves each spectrum with two identical Gaussian, one in the red wing and one in the blue wing. The separation between the two Gaussians is  $2\alpha$ . Care was taken not to include regions far out in the wings where the continuum begins to dominate by choosing reasonable values of the width ( $\sigma$ ) of the Gaussians and  $\alpha$ . Twelve standard Gaussian band-passes were used with  $\alpha$  values ranging from 3500 to 100 km s $^{-1}$  and corresponding width values from 1200 to 100 km s $^{-1}$ .

### 3.1 Period Searches

The radial velocities were Fourier transformed using the Discrete Fourier Transform (DFT) algorithm to search for any periods in the data (Deeming 1975; Kurtz 1985). The H $\beta$  and H $\gamma$  amplitude spectra from 1991 (24 and 25 April) are shown in Figure 1 and the H $\alpha$  amplitude spectra from 2001 are shown in Figure 2.

A prominent peak at a frequency corresponding to the 98-minute orbital frequency,  $\Omega$ , is observed in all the emission lines. Second in strength to the orbital frequency is the spin frequency,  $\omega$ , of the narrow s-wave component (NSC) ( $\alpha = 900, 1200$  km s $^{-1}$ ) (Figures 1 and 2). The third panels from the top in Figures 1 and 2 show the data after prewhitening by  $\Omega$ . Power at  $\omega$  is clearly present.

The spin frequency was not detected at high values of  $\alpha$  ( $\alpha = 3000, 3500$  km s $^{-1}$ ) where it is most expected (since at these velocities the material is quite close to the white dwarf and its emission is expected to be modulated at the white dwarf spin period).

It was also not present in H $\beta$  and H $\gamma$  radial velocities of 2001. The amplitude of  $\omega$  relative to  $\Omega$  was found to be  $\sim 81\%$  for H $\beta$ ,  $\sim 64\%$  for H $\gamma$  and  $\sim 18\%$  for H $\alpha$ .

## 4 ORBITAL VARIATIONS OF THE EMISSION LINES

The data were phase-binned on the orbital ephemeris of Hellier & Sprouts (1992),

$$T_{\text{eclipse}} = 2437699.94179 + 0.068233846(4)E, \quad (1)$$

where  $E$  is the number of orbital cycles and  $T$  is the time of mid-eclipse. This ephemeris is defined by the zero point of mid-eclipse, where minimum intensity is at phase 0.0. This means that for the radial velocities, maximum blueshift is perpendicular to the line of centres, at phase 0.75, meaning that spectroscopic phase zero occurs at the blue-to-red crossing of the emission line radial velocity curve. 40 phase bins were used to produce the radial velocities.

### 4.1 Orbital Tomograms and Trained Spectra

The H $\alpha$ , H $\beta$  and H $\gamma$  Doppler tomograms were computed using the Back Projection Method (BPM) with the application of a filter, and the Maximum Entropy Method (MEM) (Marsh & Horne 1988; Marsh 1988; Horne 1991; Spruit 1998). The BPM Doppler maps are shown in Figure 3 and those constructed using MEM are shown in Figure 4. Error in ephemerides (both orbital and spin) is sufficiently small to phase all of our data accurately on the orbital and spin cycles.

A velocity amplitude of the primary,  $K_1 = 74 \pm 2$  km s $^{-1}$  from our radial velocity measurements and that of the secondary,  $K_2 = 360 \pm 35$  km s $^{-1}$ , taken from Vande Putte et al. (2003) and Beuermann et al. (2003), were used to fix the positions of the Roche lobe and the stream trajectories on the tomograms. A secondary mass,  $M_2 = 0.10 \pm 0.01 M_{\odot}$  for EX Hya was derived from the up-to-date secondary mass-period relation of Smith & Dhillon (1998). The mass of the primary,  $M_1$ , was then determined from the above values using  $\frac{K_1}{K_2} = \frac{M_2}{M_1}$ , and was found to be  $0.50 \pm 0.05 M_{\odot}$ .

The H $\beta$ , H $\gamma$  and HeI  $\lambda 4471$  Doppler tomograms (Figure 3 and 4) show strong emission at the bright spot, some at the Roche lobe and the stream, and some from the disc. Those of H $\alpha$  also show strong bright spot emission but less or no emission from the stream. Disc emission is diminished in H $\alpha$  when compared to other emission lines, especially at higher velocities. This is more obvious in the BPM tomogram. The bright spot emission falls near the region  $(-100, 350)$  km s $^{-1}$ . Average-subtracted trailed spectra (Figure 4) show the corresponding NSC.  $\sim 1 \times 10^{-11}$  ergs cm $^{-2}$  s $^{-1}$  ( $\sim 60\text{--}70\%$ ) of the original line fluxes is contained in the average-subtracted profiles of H $\beta$  and H $\gamma$ , and  $\sim 1 \times 10^{-12}$  ergs cm $^{-2}$  s $^{-1}$  ( $\sim 80\text{--}90\%$ ) is contained in H $\alpha$  and HeI  $\lambda 4471$ . This flux is mainly due to the bright spot and the stream. The trailed spectra have been repeated over 2 cycles for clarity.

The trailed spectra of 2001 have revealed two interesting features. The first one is the asymmetry in the intensity of the s-wave (Figure 4). In H $\alpha$ , the red wing of the NSC is brighter at  $\phi_{98} \sim 0.1 - 0.3$  and seems to reach maximum brightness near  $\phi_{98} \sim 0.25$ , whereas the blue wing is dimmer in the range  $\phi_{98} \sim 0.7 - 0.9$  and seems to reach minimum brightness near  $\phi_{98} \sim 0.75$ . A similar effect is seen in the H $\beta$  and the H $\gamma$  lines, and to a lesser extent in HeI  $\lambda 4471$ . The second feature is redshifted emission extending from the NSC to high velocities ( $\sim 1000$  km s $^{-1}$ ) at early binary phases ( $\phi_{98} \sim 0.0 - 0.2$ ).

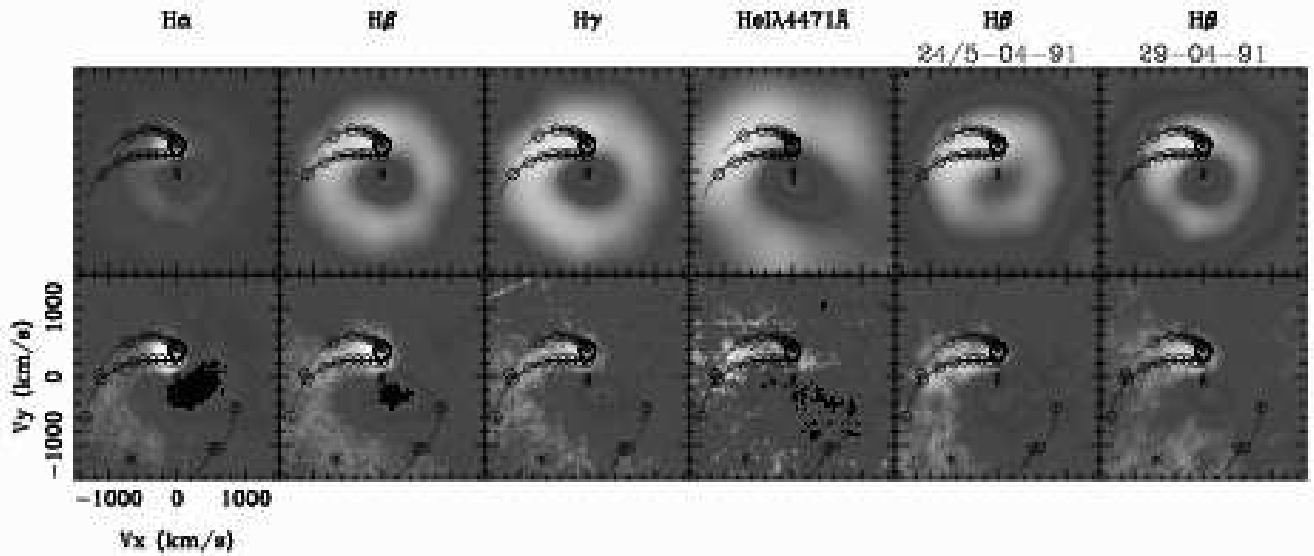


**Figure 3.** The panels show the H $\alpha$ , H $\beta$ , H $\gamma$  and HeI  $\lambda 4471$  orbital Doppler maps from 2001, and H $\beta$  tomograms of 1991, constructed using the Back-Projection Method with the application of a filter (top panels) and after subtracting the average of the line profile (bottom panels). The positions of the Roche lobe and stream trajectories are shown (velocity amplitudes of  $K_1 = 74 \text{ km s}^{-1}$  and  $K_2 = 360 \text{ km s}^{-1}$  for the primary and secondary stars, respectively, were used). The two curves with marked intervals represent the gas stream velocity (upper curve) and the Keplerian velocity along the stream (lower curve). The circles on all tomograms represent 0.1 of the distance from the  $L_1$  point to the primary. The three crosses are centres of mass of the secondary, system and primary, from top-to-bottom. The asterisk represents the velocity of closest approach. All the maps are plotted on the same velocity scale. The lookup table of this figure is such that the brightest emission features appear with decreasing intensity from yellow/green to light blue in the online edition, or white to grey in the printed edition.

The reconstructed trailed spectra suggest that this latter feature is another s-wave, which we shall refer to as the high velocity component (HVC), crossing the NSC near  $\phi_{98} \sim 0.2 - 0.3$ . The Doppler tomograms show emission extending from the bright spot position, passing along the stream path, to the bottom-left quadrant at high velocities near  $1000 \text{ km s}^{-1}$  which is responsible for the HVC; most of this emission does not fall within the disc and gas stream velocities on the map, suggesting that there was small or no overlap of the stream component with the disc.

The 1991 tomograms showed similar results. It is worth noting that most of the disc emission in 1991 came from the outer disc than in 2001.

Even though the MEM and BPM pick out the same features, in the BP tomograms some features are more prominent than in the MEM tomograms while the reconstruction obtained using the MEM reproduces the observed data well.

The advantage of BPM over MEM is that it is faster and it is easier to get a consistent set of maps of different emission lines (in terms of the apparent noise in the images). For this reason both methods have been used.

## 5 SPIN VARIATIONS OF THE EMISSION LINES

### 5.1 The Spin Radial Velocity Curve

The radial velocities were phase-folded using 30 bins on the quadratic spin ephemeris of Hellier & Sproats (1992), where spin maximum was defined as  $\phi_{67} = 0$ . Figure 5 shows the variation of the H $\beta$ , H $\gamma$  and H $\alpha$  narrow components with  $\omega$ . Maximum blueshift is seen at  $\phi_{67} = 0.79$  for H $\beta$  and at  $\phi_{67} = 0.77$  for H $\gamma$ . Whereas for H $\alpha$ , maximum blueshift is seen at  $\phi_{67} = 0.90$ . It should be noted that H $\alpha$  and H $\beta$  / H $\gamma$  have not been observed simultaneously and so

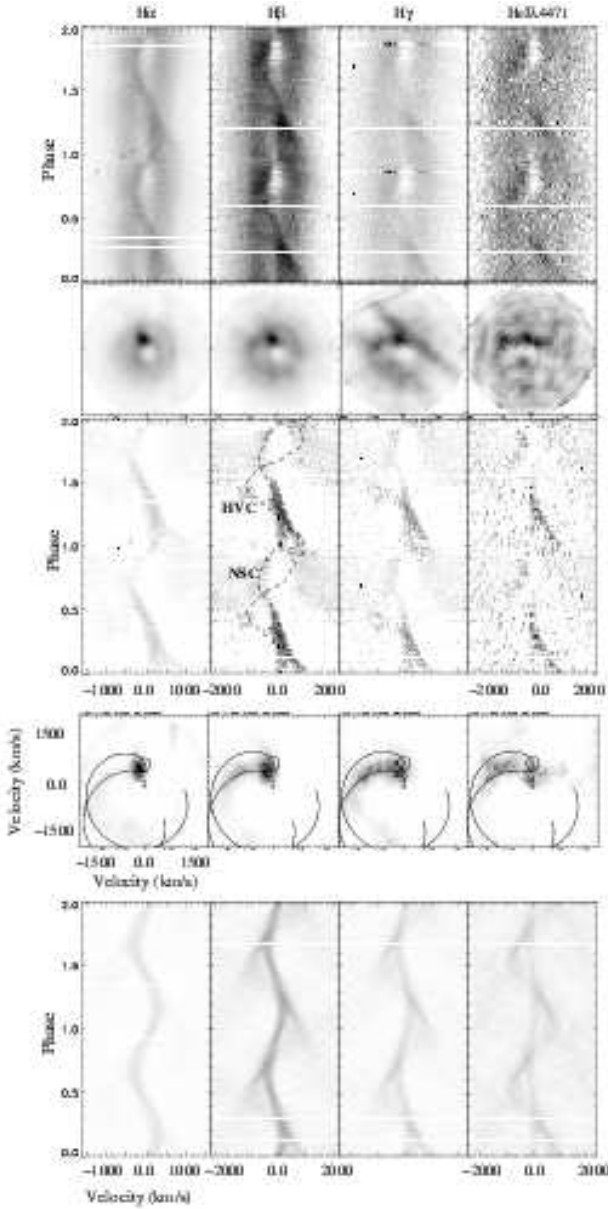
both data sets probably sample the spin phases at different orbital phases.

Figure 6 shows the H $\alpha$  narrow component ( $\alpha = 1200 \text{ km s}^{-1}$ ) and the broad-base component ( $\alpha = 3500 \text{ km s}^{-1}$ ) overplotted. The two components are in phase. The radial velocity variation with the spin period of the H $\beta$  and H $\gamma$  broad-base component could not be detected, possibly due to velocity cancellation. We discuss this in Section 6.

### 5.2 Spin Tomograms and Trailed Spectra

Spin tomograms of EX Hya were constructed by Hellier (1999) but revealed little information. Also, Belle et al. (2005) observed no coherent emission site/s on their tomograms folded on the spin phase.

The H $\beta$  and the H $\gamma$  BPM and MEM spin tomograms from 2001, however, have revealed a coherent emission site between  $V_x \sim 500 \text{ km s}^{-1}$  and  $\sim 1000 \text{ km s}^{-1}$  which is evidence of emission from the accretion curtains (Figures 7 and 8). But it is a well known fact that since the spin period is  $\sim \frac{2}{3}$  of the orbital period in EX Hya, orbital cycle variations do not smear out when folded on the spin phase but repeat every 3 spin cycles (Hellier et al. 1987). This is thought to be the origin of most of the structure in the emission lines at velocities  $< 1000 \text{ km s}^{-1}$  (Hellier 1999). To address this problem, phase-invariant subtraction is performed where emission that does not vary with the spin cycle is subtracted from the data. This is achieved by measuring minimum flux at each wavelength and subtracting this value. The results are shown in the second panels from the top of Figure 8. It should be mentioned though, that even subtracting the invariant part of the line profiles does not guarantee that the influence of the orbital period variations has been completely removed.



**Figure 4.** 2001 H $\alpha$ , H $\beta$ , H $\gamma$  and He I  $\lambda 4471$  trailed spectra (top row of panels) and MEM orbital Doppler maps (second row of panels from the top) as well as the average-subtracted trailed spectra (third row of panels) are shown plotted on the same scale except for H $\alpha$  panels. The HVC and the NSC are indicated. The fourth row shows the average-subtracted Doppler maps and the models plotted for  $q = 0.21$ ,  $i = 78^\circ$  and  $M_1 = 0.50 M_\odot$ . The bottom panels are the reconstruction of the average-subtracted data. The fourth and bottom panels are also plotted on the same scale except for H $\alpha$  panels. The lookup table of this figure is such that the brightest emission features appear with decreasing intensity from black to light grey.

A spin-wave (to differentiate it from the s-wave which is normally caused by the bright spot) in the H $\alpha$  trailed spectra (Figure 8) was detected from the data after the phase-invariant subtraction was performed. This is the first detection of modulation over the spin cycle in the optical emission line data of EX Hya. This spin-wave can be seen in the trailed spectra before (but hard to see) and after subtraction of the phase-invariant line profile. The narrow peak component is responsible for this spin-wave which is shown ex-

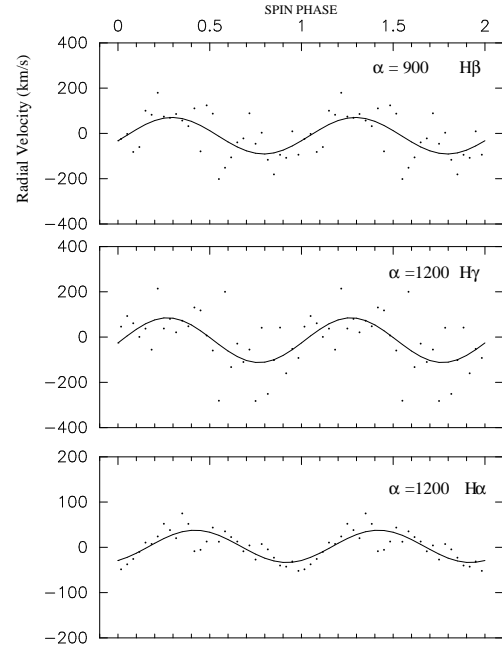


**Figure 5.** The H $\beta$  (top panel), H $\gamma$  (middle panel) and H $\alpha$  (bottom panel) spin radial velocities of the narrow component from the 1991 combined data (H $\beta$  and H $\gamma$ ) and 2001 data (H $\alpha$ ). The radial velocities were prewhitened by the orbital frequency and phase-folded on the spin frequency using 30 bins and are shown plotted as a function of the spin phase.

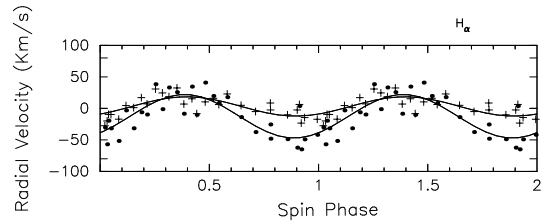


**Figure 6.** The spin radial velocity curves of the H $\alpha$  narrow (crosses) and broad (dots) components from 2001 (30 bins) plotted as a function of the spin phase. The solid line represents a fit to the data.

panded in the second column of panels in Figure 8 (the narrow peak component was selected by hand over a velocity range of  $\pm 500 \text{ km s}^{-1}$ ). The spin-wave shows maximum blueshift near phase 1.0 and maximum redshift near phase 0.5, and has an amplitude of  $\sim 500 \text{ km s}^{-1}$ . The H $\alpha$  tomogram shows corresponding emission near the “3 o’clock” position (blob of emission right at the edge of the map), around  $\sim 500 \text{ km s}^{-1}$ . DFTs show lower amplitude ( $\sim 40 \text{ km s}^{-1}$  for H $\alpha$  and  $\sim 130 - 140 \text{ km s}^{-1}$  for H $\beta$  and H $\gamma$ ) probably due to dilution by stationary material. Also, the H $\alpha$  MEM tomogram shows stronger emission that peaks in a broad structure at lower velocities ( $V_x \sim -200 \text{ km s}^{-1} - \sim +200 \text{ km s}^{-1}$  – around the “5-6 o’clock” position). Circular motion gives rise to low or zero radial velocities when the motion is perpendicular to the line of sight, and the emission seen around the “5-6 o’clock” position could not be from such velocities since it shows maximum blueshift at  $\phi_{67} \sim 0.2 - 0.25$ . Similar emission was observed in a Polar and was thought to be due to material that has just been decelerated after having attached to the magnetic field lines (Schwarz et al. 2005) (we discuss an alternative explanation in Section 6). The emission near the edge

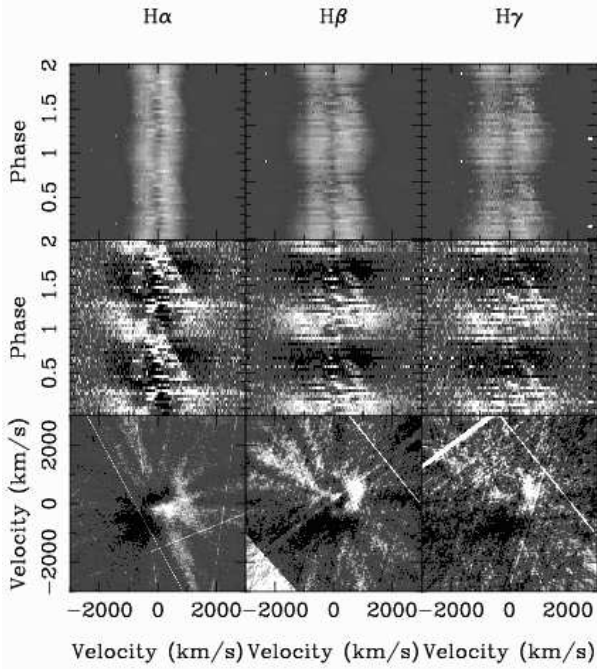


**Figure 7.** The H $\alpha$ , H $\beta$ , H $\gamma$  and HeI  $\lambda 4471$  trailed spectra from 2001 folded on the spin period are shown at the top panels and the average-subtracted spectra are shown at the second panels. Doppler maps constructed from the phase-invariant subtracted spectra are shown in the bottom panels. The Doppler maps were constructed using the BPM and are shown on the same velocity scale with the trailed spectra. The lookup table is as in Figure 3.

of the tomogram (at  $\sim 500 \text{ km s}^{-1}$ ) shows maximum blueshift at  $\phi_{67} \sim 1.0$  and therefore cannot be due to motion perpendicular to the line of sight either.

The H $\alpha$  trailed spectra also show emission coupled to the spin-wave near  $\phi_{67} \sim 0.1 - 0.6$  that extends to high velocities in the red, a similar situation to that seen in the orbital tomograms due to the HVC (Section 4.1). The corresponding emission in the H $\alpha$  tomograms extending to higher velocities in the red spectral region is not clear.

Both the H $\beta$  and H $\gamma$  phase-invariant subtracted trailed spectra show three weak-intensity spin-waves. The most clearly visible of the three is phased with maximum redshift near  $\phi_{67} \sim 0.3 - 0.4$ , with an estimated velocity amplitude of  $\sim 900 \text{ km s}^{-1}$  and corresponds to the emission near the “3 o’clock” position in the tomogram (Figure 8). The reconstructed trailed spectra reproduce the observed data.

The H $\beta$  and H $\gamma$  trailed spectra in Figure 7 seem to support these results. The emission observed near the “3 o’clock position” in the tomograms has also been seen in other IPs such as AO Psc and FO Aqr (Hellier 1999) and was interpreted as emanating from the upper accretion curtain.

The spin-waves are weak in intensity though, and more data are needed to support these results.

## 6 DISCUSSION OF THE ORBITAL AND SPIN DATA

The generally accepted model of EX Hya has the material leaving the secondary star through the  $L_1$  point, passing via a stream of material which orbits about the white dwarf, to form an accretion

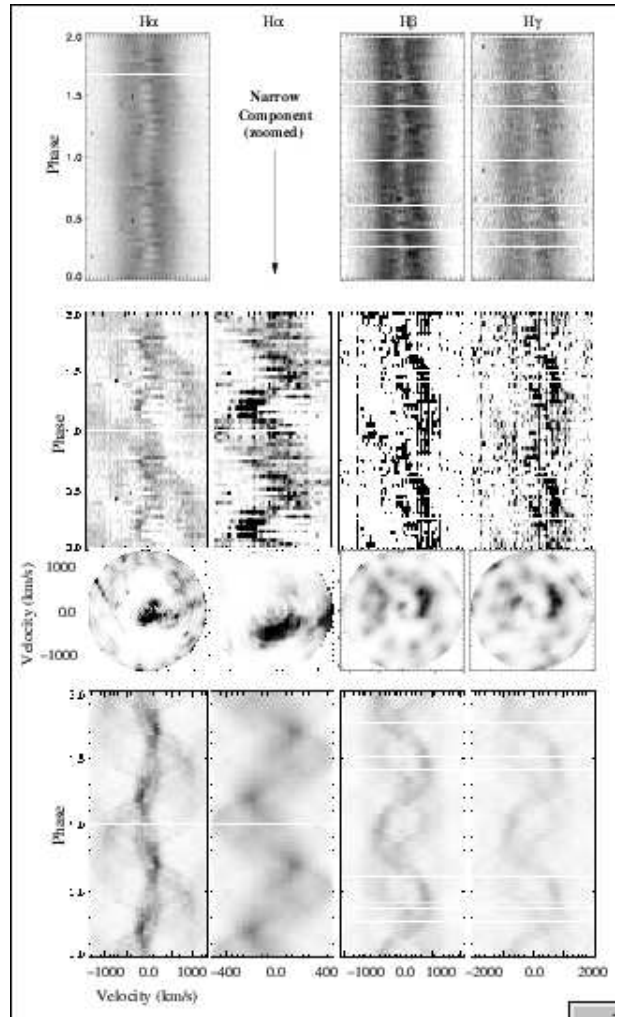


**Figure 8.** H $\alpha$ , H $\beta$  and H $\gamma$  trailed spectra of 2001 folded on the spin period are shown in the top panels and the phase-invariant subtracted trailed spectra are shown in the second panels from the top. MEM spin Doppler tomograms constructed from the phase-invariant subtracted spectra are shown in the third panels with the reconstructed spectra in the bottom panels. The spin wave observed in the H $\alpha$  phase-invariant subtracted trailed spectra, which was caused by the H $\alpha$  narrow component, is shown expanded on a smaller velocity scale. The first column of panels are plotted between  $-1500 \text{ km s}^{-1}$  and  $1500 \text{ km s}^{-1}$  and the last two columns are plotted between  $-2000 \text{ km s}^{-1}$  and  $+2000 \text{ km s}^{-1}$ . The lookup table is as in Figure 4.

disc. The magnetic field lines of the white dwarf which form accretion curtains above and below the orbital plane channel the material from the disc, starting from the co-rotation radius ( $R_{co}$ ) where the disc is truncated by the field lines, to the surface of the white dwarf (Hellier et al. 1987; Rosen et al. 1991).

King & Wynn (1999) challenged this model by arguing that systems with  $P_{spin}/P_{orb} > 0.1$  cannot possess Keplerian discs since this implies  $R_{co} \gg R_{cir}$ . They showed that the spin equilibrium state in EX Hya is determined by  $R_{co} \sim b$ , where  $b$  is the distance to the  $L_1$  point. In this model the accretion curtains extend to near the  $L_1$  point, and EX Hya resembles an asynchronous polar where most of the material accretes via the stream (King & Wynn 1999; Wynn 2000).

Belle et al. (2002) revised the model of EX Hya after they showed that their EUV data support the model of King & Wynn

(1999). Their revised model suggested that the magnetic field in EX Hya forms a large accretion curtain extending to the outer edge of the Roche lobe causing:

- part or all of the non-Keplerian disc (hereafter the ring of material or the ring) to rotate with the white dwarf,
- an extended bulge (later, Belle et al. (2005) showed that there was Vertically Extended Material (VEM) obscuring the s-wave emission during  $\phi_{98} = 0.57 - 0.87$ , and evidence for overflowing stream accretion in EX Hya), and
- the ring of material to feel magnetic force at the regions of the ring close to the poles, causing the ring material at these locations to be controlled by the magnetic field, forming two chunks along the accretion ring that rotate with the white dwarf.

Recently, Norton et al. (2004, 2004a) have shown that for systems with  $P_{spin}/P_{orb} \sim 0.72$ , when the mass ratio is smaller at  $q = 0.2$ , the material forms a ring near the edge of the primary Roche lobe, from where accretion curtains funnel down to the white dwarf surface, in agreement with King & Wynn (1999) and Belle et al. (2002). The material is fed from the ring (ring-fed accretion) and channeled along the magnetic field lines (when the angle between the white dwarf spin axis and magnetic dipole axis is small i.e.  $\epsilon < 30^\circ$ , which is true for EX Hya).

The discussion by Eisenbart et al. (2002) on the IR-UV flux distribution in EX Hya implies a disc (isobaric and isothermal) with an outer radius of  $1.6 \times 10^{10}$  cm and a thickness of  $2 \times 10^8$  cm, and an assumed central hole of  $6 \times 10^9$  cm, but Eisenbart et al. (2002) suggested that the structure could also be a ring with a larger inner radius, in line with the suggestion of King & Wynn (1999); Belle et al. (2002) and Norton et al. (2004). They found that the disc component contains about 1/6 of the total flux which is a bit more than expected from gravitational energy release at the inner radius,  $R_{in} > 6 \times 10^9$  cm.

Our spectroscopic data support both the model of Belle et al. (2002) and Norton et al. (2004) in which material from a ring, circling the white dwarf and co-rotating with the magnetic field lines at the outer edge of the Roche lobe, is accreted by the white dwarf.

The presence of the bright spot revealed by the trailed spectra, the DFTs of the radial velocities and the Doppler maps (Figures 3 and 4) suggest the presence of a disc or ring of material extending to near the Roche lobe radius, around the white dwarf. When comparing the 1991 and 2001 tomograms for the H $\beta$  they appear to be in the same state or similar, given the fact that they are ten years apart. It is reassuring that the fact that the two groups of lines have not been measured simultaneously is not a significant problem in the analysis.

More importantly, a spin pulse modulated at velocities consistent with those of the material circulating at the outer edge of the disc ( $\sim 500 - 600$  km s $^{-1}$ ) (Figures 1 and 2) was detected and provides evidence for co-rotation of the extended accretion curtains with the ring material. As discussed in Section 5.2, these low radial velocities mentioned above were not caused by motion perpendicular to the line of sight near the white dwarf, neither were they caused by velocity cancellation as will be shown later.

A spin wave was detected in the spin-folded trailed spectra of H $\alpha$  (Figure 8) with a velocity semi-amplitude of  $\sim 500$ - $600$  km s $^{-1}$ . The spin wave shows maximum blue-shift near phase  $\phi_{67} \sim 1.0$  (when the upper magnetic pole is pointed away from the observer) and maximum redshift near phase  $\phi_{67} \sim 0.5$ . The H $\alpha$  equivalent widths show maximum flux near  $\phi_{67} \sim 1.0$ . This picture is consistent with the accretion curtain model of IPs and is possible if accretion occurs via a disc/ring. The spin tomograms (Figures 7

and 8) show evidence of the accretion curtain emission extending from  $\sim 500$  km s $^{-1}$  to high velocities ( $\sim 1000$  km s $^{-1}$ ), suggesting that material is channeled along the field lines from the outer ring. The H $\alpha$  narrow and broad base components show similar phase variation, suggesting same position of maximum radial velocity as shown in Figures 6 and 9 (line OA). This indicates that material is channeled from the ring (at low velocities) to high velocities along the field lines.

A mass ratio of  $q \sim 0.2$  was measured from our data, and so the period ratio  $P_{spin}/P_{orb} \sim 0.68$  is consistent with the ring accretion model of Norton et al. (2004).

Decreased prominence of the narrow s-wave component around  $\phi_{98} = 0.57 - 0.87$  (Figure 3 and 4) was observed and suggests the presence of VEM at the outer edge of the ring of material obscuring the emission at these phases. The presence of the overflow stream may be inferred from this observation (Belle et al. 2005). But direct evidence comes from orbital Doppler tomograms which show an asymmetry in the emission, where more emission is observed from the secondary Roche lobe to the lower left quadrant than from the opposite side. Average-subtracted orbital tomograms show this emission at higher velocities ( $\sim 900$ - $1000$  km s $^{-1}$ ) (Figures 3 and 4), and it corresponds to the HVC observed in the trailed spectra, which is modulated with a velocity semi-amplitude of  $\sim 1000$  km s $^{-1}$ . This HVC is reminiscent of that detected by Rosen et al. (1987) in the trailed spectra of the AM Her system V834 Cen. Their HVC was blueshifted with a velocity of  $900$  km s $^{-1}$  and was said to be produced in the stream close to the white dwarf. The only difference is that there was no evidence of the HVC emission when it was expected to be seen redward of another component (medium-velocity component) in their data, whereas in EX Hya the evidence of the HVC emission is missing between  $\phi_{98} \sim 0.3 - 0.85$ . The HVC emission is maximally blueshifted at  $\phi_{98} \sim 0.3 - 0.4$ . This phasing is consistent with the expected phase of impact of a stream of material from the secondary with the disc or of the overflow stream material free-falling onto the magnetosphere of the primary (Hellier et al. 1989).

Support for overflow stream is also provided by spin tomograms where emission is observed on the upper accretion curtain with velocities consistent with stream velocities. This suggests that this emission site may also have resulted due to impact of overflow stream with the magnetosphere. The resulting emission is receding from the observer at maximum redshift near  $\phi_{67} \sim 0.4$  (Figure 8), in agreement with the accretion curtain model.

The model of King & Wynn (1999) is not fully supported by our observations since it predicts direct accretion via a stream. Our observations, however, fit the models of Norton et al. (2004) and Belle et al. (2002, 2005). There is evidence for strong H $\alpha$  emission of the narrow s-wave component in the spin tomograms, centred around  $\sim 100$  km s $^{-1}$  (Figure 8), that is not accounted for by these models. This emission shows maximum blueshift at phase  $\phi_{67} \sim 0.2$ , suggesting that these are rotational velocities (or a combination of streaming and rotational velocities) of the antiphased motion of a source locked to the white dwarf. One possible explanation is that this emission comes from the opposite pole of the white dwarf, at a radial distance of  $6 \times 10^9$  cm ( $\sim 8R_{wd}$ ). Siegel (1989) found that the eclipsed optical source in EX Hya is centred at a radial distance of  $1.5 \times 10^9$  cm ( $\sim 2R_{wd}$ ), which is about four times closer to the white dwarf compared to our result. This could be the same emission region, but in our observations the emission is spread out, possibly due to the quality of the data, and this could account for the difference in the radial distance values quoted above. But we cannot imagine a geometry where such low rotational ve-

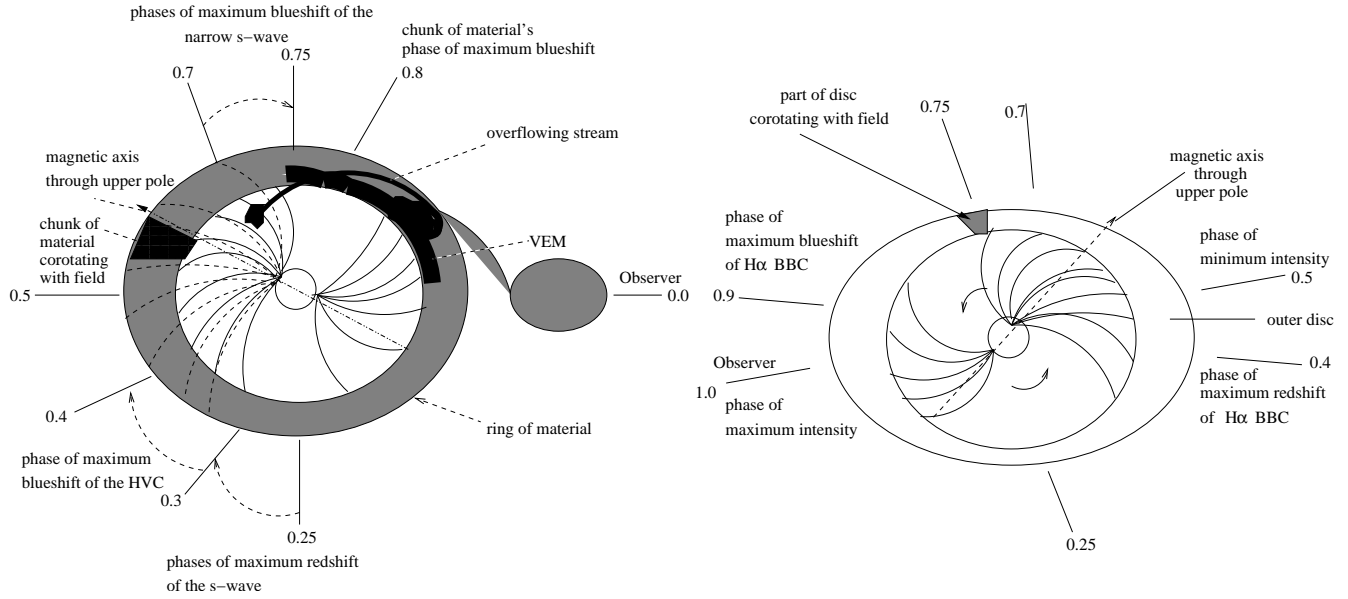


**Figure 10.** A model of EX Hya in quiescence. The figures are drawn over the orbital cycle (left) and spin cycle (right) and show the magnetosphere extending to the outer edge of the ring, and the chunk of material corotating with the field lines. A vertically extended material (VEM) is irradiated by the white dwarf in its inner regions (left).

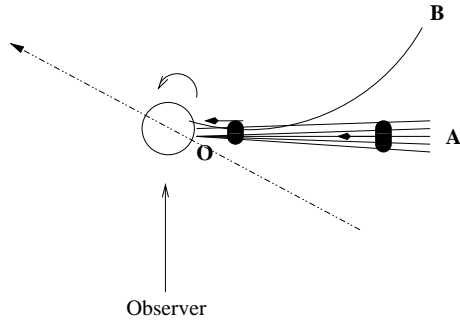


**Figure 9.** A depiction of the regions where H $\alpha$  was formed. Both the narrow and broad base components fall along the same radial direction, OA, resulting in similar phase variation.

locities can dominate over streaming velocities along the field lines near the white dwarf. We therefore suggest that this is evidence for material that is diverted out of the orbital plane. Since one of the assumptions of Doppler tomography is that everything lies on the plane, it is not possible to locate the exact position of this emission relative to the white dwarf.

### 6.1 White dwarf and secondary masses

Hellier et al. (1987) showed that maximum line widths of  $\pm 3500$  km s $^{-1}$  constrain the mass of the white dwarf, and a free-fall velocity of this magnitude could be achieved for white dwarf masses greater than  $0.48 M_{\odot}$ . We found  $M_1 = 0.50 \pm 0.05 M_{\odot}$ , in good agreement with the results obtained from recent studies by Hoogerwerf et al. (2004); Beuermann et al. (2003) and Vande Putte et al. (2003).

For the secondary, we derived  $M_2 = 0.10 \pm 0.01 M_{\odot}$  from the secondary mass-period relation of Smith & Dhillon (1988), and this value agrees with that obtained by Vande Putte et al. (2003).

Beuermann et al. (2003) and Hoogerwerf et al. (2004) find lower values for  $M_2$  consistent with  $0.09 M_{\odot}$ . Eisenbart et al. (2002) argues that for a secondary mass as low as  $0.1 M_{\odot}$  the secondary would have to be substantially expanded by  $\sim 10\%$ .

### 6.2 The revised model of EX Hya

We propose a model where one of the two chunks alluded to by Belle et al. (2002), which are formed by the magnetic pull along the accretion ring, co-rotates with the accretion curtains at the outer edge of the Roche lobe at  $\sim 500$ – $600$  km s $^{-1}$ , giving rise to the pulsation of emission at the spin period which we observe in our data, while the other is hidden by the accretion curtain below the ring of material. The resulting emission is maximally blueshifted near  $\phi_{67} \sim 0.8$  (Figure 5). In the accretion curtain model, at  $\phi_{67} \sim 0.5$  in the spin cycle, minimum flux (due to higher opacity) is observed when the upper accretion pole of the white dwarf is pointed towards the observer (Hellier et al. 1987), and so the phasing mentioned above is compatible with the motion of a rotating accretion funnel. This is illustrated in Figure 10, where the position of the observer at pulse maximum is indicated, and the axis of the magnetic pole is shown. The disruption of the disc by the magnetic field at the outer disc is illustrated and part of the disc co-rotating with the magnetosphere is shown. At a corotation radius,  $R_c \sim b = a(0.500 - 0.227 \log \frac{M_2}{M_1})$  ( $\sim 3 \times 10^{10}$  cm), the material is rotating at a velocity of  $v^2 = \frac{GM}{b} \sim 500$  km s $^{-1}$ , in good agreement with the observations. Also, a rotation velocity of  $\sim 600$  km s $^{-1}$  was measured from the spectra and the radial distance from the star to the ring of material was found to be  $\sim 3 \times 10^{10}$  cm, which is similar to  $b$ , for a white dwarf mass of  $0.5 M_{\odot}$  (Keplerian motion about the white dwarf had to be assumed in these calculations). At this radius, the accretion curtain is also rotating at a velocity of  $2\pi R_{co}/P_{spin} \sim 500$  km s $^{-1}$ .  $\sim 6 \times 10^{-12}$  ergs cm $^{-2}$  s $^{-1}$  (64% - integrated over one spin cycle) of the original line fluxes that is contained in the average-



subtracted profile of H $\alpha$  shows radial velocity variations with the spin period. Assuming that H $\beta$  and H $\gamma$  also show a similar flux variation (H $\beta$  and H $\gamma$  spin tomograms also show a low-velocity s-wave but this result is not secured due to poor quality of data), the total line fluxes showing radial velocity variations with the spin period can be estimated to be  $\sim 2 \times 10^{-11}$  ergs cm $^{-2}$  s $^{-1}$  for the three emission lines. This is  $\sim 2/10$  of the total disc flux (Eisenbart et al. 2002), suggesting that only part of the ring corotates with the white dwarf while the rest of the material may be involved in a near Keplerian motion (this is a rough comparison since the flux is integrated over one spin cycle for H $\alpha$ , H $\beta$  and H $\gamma$  in our data whereas Eisenbart et al. (2002) derived their total flux values from one spectrum over the wavelength range  $\lambda = 912 - 24000$  Å).

While some of the ring material co-rotates with the accretion curtains (i.e. remains in the disc rather than being immediately channelled along the field lines), some is channelled along the field lines at  $\sim 500$  km s $^{-1}$  towards the white dwarf. There is also some material that overflows the ring and attaches onto the magnetic field lines. The overflow stream hits the magnetosphere, probably causing a second bright spot on the slowly rotating magnetosphere (Figure 10). The overflow stream is irradiated by the white dwarf in its inner regions close to the white dwarf (the regions facing the white dwarf). This results in the HVC emission being obscured at  $\phi_{98} \sim 0.4 - 0.9$ , which are phases where the stream is viewed from behind-opposite the side facing the white dwarf, hiding the irradiated inner regions. HVC emission from the stream is blueshifted when that from the narrow s-wave component shows maximum redshift. Near  $\phi_{98} \sim 0.25$  the two s-waves intersect, explaining the asymmetry in the brightness of the s-wave seen near  $\phi_{98} \sim 0.25$  (Figure 4). The overflow stream curls nearly behind the white dwarf and it is truncated by the field when the upper magnetic pole is facing the stream.

Ferrario & Wickramasinghe (1993) and Ferrario, Wickramasinghe & King (1993) showed that in IPs the accretion curtain below the orbital plane can contribute in the radial velocities of a system if it can be seen either through the central hole of the truncated disc, or from below the disc, or both. This effect will result in velocity cancellation due to nearly equal quantities of material that are blueshifted and redshifted on the accretion curtains (Ferrario, Wickramasinghe & King 1993).

In EX Hya where the inclination is high ( $78^\circ$ ) and the disruption radius is large ( $\sim 40 R_{WD}$ , for a white dwarf mass of  $0.5 M_\odot$ ) as proposed in Figure 10, it is clear that we see spin-varying emission from two opposite magnetic poles, producing a fairly symmetric structure in the spin-folded line profiles (Hellier et al. 1987; Rosen et al. 1991). If emission from these opposite poles is cancelling out then the sum will have a much lower velocity. This could explain the near zero and low amplitude of the radial velocity variation at the spin period of the H $\beta$  and H $\gamma$ , and H $\alpha$  ( $\leq 40$  km s $^{-1}$ ) broad-base component, respectively (see also Hellier et al. (1987) and Ferrario, Wickramasinghe & King (1993)).

One could take this argument further by suggesting that the spin modulation we observe in our data at velocities near  $\sim 500$  km s $^{-1}$  (Figures 1 and 2) is just the slight asymmetries between the two poles. The resulting velocity could just be a measure of the degree to which the poles cancel their velocities near  $\pm 3500$  km s $^{-1}$  (Coel Hellier; private communication). This, however, cannot be the case for H $\beta$  and H $\gamma$  since these two emission lines show motion that is consistent with that of a rotating object, suggesting that the line profiles are not dominated by the infall velocities at the two opposite accretion poles. If they were produced close to the white dwarf then maximum rotational velocity near  $\pm 3500$  km

s $^{-1}$  would be  $2\pi R/P_{spin} \sim 30$  km s $^{-1}$ , which is much smaller than  $\sim 500$  km s $^{-1}$ . However, rotational velocities close to the ring are  $\sim 500$  km s $^{-1}$ . For H $\alpha$ , however, we observe maximum blueshift at  $\phi_{67} \sim 1.0$ , and so velocity due to cancellation anywhere between 0 and  $\pm 3500$  km s $^{-1}$  are expected, depending on how much the two poles cancel. If both accretion curtains are still visible and symmetric at large radii (which is possible as suggested by Ferrario, Wickramasinghe & King (1993) and our model), velocity cancellation will still result in smaller amplitudes than those of  $\sim 500$  km s $^{-1}$  observed in our data. This would then count against the argument above. Furthermore, H $\alpha$  orbital Doppler tomograms show strong emission at the bright spot. If our model is correct, the field lines should also attract this H $\alpha$  dominated material, which is channelled along the field lines, as already shown above. The velocity of this material due to streaming motion near the outer ring is less than that of the H $\alpha$  broad-base component close to the white dwarf, as expected. A strong constraint on our model is that the disruption radius of EX Hya has been shown to be at  $5.9 \times 10^9$  cm (Hellier et al. 1987; Beuermann et al. 2003) which implies a white dwarf magnetic moment of  $\mu \sim 7 \times 10^{31}$  G cm $^3$ . For our model this would imply that the accretion curtains do not extend to near the Roche lobe radius. The theoretical analysis of King & Wynn (1999) and Wynn (2000), however, has shown that equilibrium rotation is possible if the magnetic moment in EX Hya falls within the range of  $10^{33} \leq \mu \leq 10^{34}$  G cm $^3$ . These are comparable to weakest field AM Hers below the period gap, and that EX Hya could possess such magnetic moments is supported to a certain extent by the average-subtracted trailed spectra of EX Hya that are reminiscent of emission lines seen in some Polars, e.g. V834 Cen (as discussed above), EF Eri (Crampton et al. 1981; Cowley et al. 1982), QS Tel (Romero-Colmenero et al. 2003) and VV Pup (Diaz 1994). Furthermore, Cumming (2002) raised the possibility that the magnetic fields in IPs are buried by the material due to high accretion rates and so are not really as low as they appear. The ring structure in EX Hya could imply higher accretion rates in EX Hya than previously thought since the capacity of the ring of material to store matter may be low when compared to that of a classical disc, resulting in the accretion of more material than in a classical disc case.

## 7 SUMMARY

Optical observations of EX Hya and the analysis have suggested that large accretion curtains extending to a distance close to the  $L_1$  point exist in this system. The DFTs and spin tomograms have for the first time provided evidence for corotation of the field lines with the ring material near the Roche lobe. Also, tomography and the phasing of the spin waves have suggested that feeding by the accretion curtains of the material from the ring (ring-fed accretion) takes place. These findings support the models of Belle et al. (2002) and Norton et al. (2004) for EX Hya and the simulations done by Norton et al. (2004a) which have shown that for systems with the parameters of EX Hya, the accreting material forms a ring at the outer edge of the primary Roche lobe, from where accretion curtains funnel down to the white dwarf surface.

Evidence for stream overflow accretion has been observed. The HVC caused by the overflow stream disappeared at  $\phi_{98} \sim 0.4 - 0.9$  due to obscuration by the stream. Obscuration of the NSC at  $\phi_{98} \sim 0.57 - 0.87$  suggested the presence of the VEM which was irradiated by the white dwarf in its inner regions.

The H $\alpha$  broad-base component shows a radial velocity variation with the spin period whereas that of H $\beta$  and H $\gamma$  could not be

detected. The low-amplitude velocity variations modulated at the spin period for H $\alpha$  and for H $\beta$  and H $\gamma$  is explained in terms of velocity cancellation effects.

We have provided an explanation for the asymmetry in the intensity of the narrow s-wave component seen in EX Hya trailed spectra in the optical. The narrow s-wave component and the HVC cross at  $\phi_{98} \sim 0.25$ , resulting in the asymmetry in brightness that we observe at these phases.

The spin-folded trailed spectra are not of good quality and more data are needed to confirm these results.

## ACKNOWLEDGMENTS

NM would like to acknowledge financial support from the Sainsbury/Linsbury Fellowship Trust and the University of Cape Town. We would like to thank Kunegunda Belle, Coel Hellier and Andrew Norton for invaluable discussions and for their constructive comments. We acknowledge use of D. O'Donoghue's and Tom Marsh's programs Eagle and Molly, respectively.

## REFERENCES

- Belle, K., Howell S. B., Sirk, M., Huber, M.E., 2002, *ApJ*, 577, 359
- Belle, K., Howell, S., Mukai, K., Szkody, P., Nishikida, K., Ciardi, D.R., Fried, R.E., Oliver, J.P., 2005, *ApJ*, 587, 373
- Beuermann, K., Harrison, Th. E., McArthur, B. E., Benedict, G. F., Gansicke, B.T., 2003, *A&A*, ms3775
- Buckley, D., Schwarzenberg-Czerny, A., 1991, Cataclysmic Variable and Related Physics, 2nd Technion Haifa Conference, *Annals of the Israel Physical Society*, 10
- Cowley, A.P., Crampton, D., Hutchings, J.B., 1982, *ApJ*, 259, 370
- Crampton, D., Hutchings, J.B., Cowley, A.P., 1981, *ApJ*, 243, 567
- Cumming, A., 2002, *MNRAS*, 333, 589
- Deeming, T. J., 1975, *Ap&SS*, 36, 137
- Diaz, M. P., Steiner, J. E., 1994, *A&A*, 283, 508
- Eisenbart, S., Beuermann, K., Reinsch, K., Gansicke B.T., 2002, *A&A*, 382, 984
- Ferrario, L., Wickramasinghe, D., 1993, *MNRAS*, 265, 605
- Ferrario, L., Wickramasinghe, D., King, A., 1993, *MNRAS*, 260, 149
- Hellier, C., Mason, K., Rosen, R., 1987, *MNRAS*, 228, 463
- Hellier, C., Mason, K., Smale, A. P., Corbet, R. H. D., O'Donoghue, D., Barrett, P. E., Warner, B., 1989b, *MNRAS*, 238, 1107
- Hellier, C., Sproats, L. N. 1992, *IBVS*, 3724
- Hellier, C., 1999, *ApJ*, 519, 324
- Hoogerwerf, R., Brickhouse, N. S., Mauche, C. W., 2004, *ApJ*, 610, 411
- Horne, K., 1991, in: *Fundamental Properties of Cataclysmic Variable Stars: 12th North American Workshop on Cataclysmic Variables and Low Mass X-ray Binaries*, San Diego State University Publication, San Diego, ed. A.W. Shafter, 23
- King, A., Wynn, G. A., 1999, *MNRAS*, 310, 203
- Kurtz, D. W., 1985, *MNRAS*, 213, 773
- Marsh, T. R., 1988, *MNRAS*, 231, 1117
- Marsh, T. R., Horne, K., 1988, *MNRAS*, 235, 269
- Mumford, G., 1967, *ApJS*, 15, 1
- Norton, A., Wynn, A., Somerscales, C., 2004, *ApJ*, 614, 349
- Norton, A., Somerscales, R. V., Parker, T. L., Wynn, A., West, R., 2004a, *RevMexAA*, 20, 138
- Romero-Colmenero, E., Potter, S., Buckley, D., 2003, *Astrotomography*, 25th meeting of the IAU, Joint Discussion 9, 17 July 2003, Sydney, Australia
- Rosen, S.R., Mason, K.O., Cordova, F.A., 1987, *MNRAS*, 224, 987
- Rosen, S.R., Mason, K.O., Mukai, K., Williams O.R., 1991, *MNRAS*, 249, 417
- Schneider, D.P., Young, P., 1980, *ApJ*, 238, 946
- Schwarz, R., Schwöpe, A.D., Staude, A., Remilland, R. A., 2005, *A&A*, 444, 213
- Shafter, A.W. 1983, *ApJ*, 267, 222
- Shafter, A.W., Szkody, P., 1984, *ApJ*, 276, 305
- Shafter, A.W. 1985, *Cataclysmic Variables and Low-Mass X-Ray Binaries*, D.Q. Lamb and J. Patterson (eds), 355, 358
- Siegel, N., Reinsch, K., Beuermann, K., van der Woerd, H., Wolff, E., 1989, *A&A*, 225, 97
- Smith, D. A., Dhillon, V. S., 1998, *MNRAS*, 301, 767
- Spruit, H. C., 1998, preprint(astro-ph/9806141)
- Vande Putte, D., Smith, R. C., Hawkins, N. A., Martin, J. S., 2003, *MNRAS*, 342, 151
- Wynn, G. A., 2000, *New Astr. Rev.*, 44, 75